https://doi.org/10.1016/j.desal.2019.114101

Thermodynamic investigation and optimization of a heat pump coupled open-air, open-water humidification dehumidification desalination system with a direct contact dehumidifier

Weifeng He*[1,2], Hongxing Yang[1], Dong Han[2]

1. Renewable Energy Research Group (RERG), Department of Building and Services Engineering, The Hong Kong Polytechnic University, Hong Kong, China

2. Energy Conservation Research Group (ECRG), College of Energy and Power Engineering, Nanjing University of Aeronautics and Astronautics, Nanjing, 210016, China

Corresponding author: W.F. He

The Hong Kong Polytechnic University

Hung Hom, Kowloon, Hong Kong

Tel./Fax numbers: +852 27665863

E-mail address: wfenghe@polyu.edu.hk, wfhe@nuaa.edu.cn

ABSTRACT: This paper focuses on a novel heat pump powered desalination system (HPPDS), in which the heat pump is coupled into the humidification dehumidification (HD) desalination subsystem with open-air, open-water (OAOW) configurations. Based on the conservation equations in accordance with the flow streams within the system, thermodynamic investigations, at the energetic and entropic viewpoints, are conducted. Thereinto, parametric analysis of the HPPDS is first achieved to assess the influence extents from the critical conditions, and then the thermodynamic optimization based on the algorithm of particle swarm optimization (PSO) is also completed. The research results indicate the best performance of the HPPDS reaches 89.27kgh^{-1} for the water production and 4.17 for the gained-output-ratio (GOR). The performance of the HPPDS is very sensitive to the alternation of the prescribed parameters, except the dehumidification effectiveness. Finally, the maximum water production and GOR can be optimized to 150.75kgh^{-1} and 8.12, respectively, and a fully coupled HPPDS is

acquired without a auxiliary heater. According to the comparison of desalination performance between the current and the previous investigated configuration, it is found that the HPPDS with a direct contact dehumidifier has obvious advantages at the aspect of energy conservation, compared to the system with a surface dehumidifier.

Keywords: heat pump; humidification dehumidification; open-air, open-water configuration; parametric analysis; particle swarm optimization

Nomenclature

Roman symbols	
i	specific enthalpy (kJkg^{-1})
I	enthalpy difference (kW)
i_{fg1}	latent heat of the produced water during dehumidification (kJkg^{-1})
i_{fg2}	latent heat of the produced water during evaporation (kJkg^{-1})
m	mass flow rate (kgs^{-1})
Q	heat load (kW)
s	specific entropy (kJkg^{-1}K^{-1});
S	entropy rate (kJs^{-1}K^{-1}); concentration of seawater (gkg^{-1})
T	temperature (K)
W	compression power consumption (kW)
Greek letters	
ε	humidification and dehumidification effectiveness
φ	relative humidity
ω	humidity ratio (gkg^{-1})
Subscripts	
a	ambient
b	brine
c	compressor
con	condenser
d	dehumidifier
da	dry air
e	evaporator
gen	generation
h	humidifier; heater
i	inlet
m	middle
o	outlet
r	refrigerant
re	recuperator
sw	seawater

t	total
v	valve
w	water

1. Introduction

As a promising pattern of desalination, humidification dehumidification method, simulating the water cycle in the environment, has attracted extensive attention all over the world [1-3]. Early in 1996, the superiority of the HD desalination was validated by Farid [4], through establishing a HD desalination system with a flat plate solar collector to heat the seawater. In the HD desalination system, the daily water production arrived at 12kgm^{-2}, which was much more prominent compared to single basin still. Furthermore, it was discovered that the heat recovery process, involved in the condensation of the humid air, contributed to the high thermal efficiency of the entire HD desalination system.

Recent years, in view of the validated superiority of desalination performance, the research in the field of HD desalination system has been the focus topic all over the world [5, 6]. A double-stage indirect solar dryer with reheating frames was coupled into a HD desalination systems by Kabeel [7]. Based on the established experimental platform, the performance of the HD desalination unit was tested. The experimental results showed that the water production increased from 29.55 to 42.3 L per day. At the aspect of the GOR, it varied over the ranges of 1.24 to 1.79 and 0.97 to 1.38 for the coupled and single HD desalination system, and an elevation of 29% for the energy conversion efficiency was obtained through increasing the mass flow rate of the cycling air. A novel HD desalination system, with a half open-air, open-water configurations, was proposed by Mahdizade [8]. The thermodynamic analysis as well as the performance enhancement at the designated top temperatures of the novel HD desalination system was completed. Compared to the previous configurations, the energy conversion efficiency was raised significantly due to the elevation of the GOR. Campos [9] also proposed a HD desalination system, with saturated air cycling within the system. Critical parameters were first investigated to explore the performance optimization for the acquired temperature. Based on the validated mathematical models, the parametric analysis

was achieved to determine the relations between the input conditions and water production. It was concluded that the humidifier height, heat load of the solar heater and the mass flow rate of the cycling seawater were the most significant factors to determine the water production, while the relevant influence from the ambient temperature was very limited.

In addition of the extensive investigation on the simple HD desalination system, various methods were also advised to optimize the general system [10]. The variable pressure configurations of the HD desalination system was introduced to improve the desalination performance [11-13]. As known based on the thermodynamics, the carried capacity of steam in the air can be raised a lot in vacuum environment compared to that in the ambient pressure. Hence, the humidification was achieved in a lower pressure, and then the humidified air was compressed and dehumidified. Hence, the water production as well as the GOR was optimized with the variable pressure schemes. Extraction and injection [14-16] were another effective way to improve the desalination performance. In view of a significant irreversible loss in the general HD unit, single or multiple extraction and injection was introduced to balance the humidification and dehumidification processes, and the desalination performance can be improved a lot. Taking the single extraction and injection into the general closed-air HD desalination system for instance, the recovery ratio from the feed seawater and GOR were elevated to 11% and 14 from 7% and 3.5, respectively, which indicated the great potential to improve the energy conversion efficiency in the HD desalination field. Furthermore, due to the obvious superiority of the energy conservation performance from the heat pump application in the industry [17], the coupled system with the HD and heat pump was also proposed to optimize the desalination performance [18, 19]. A combined system, with a water-heated HD desalination system and heat pump coupled, was first proposed by He [20], in which the condenser was applied to raise the temperature of the sprayed seawater while the evaporator was applied to cool the concentrated brine at the bottom of the humidifier. After the thermodynamic analysis, it was found that the water production and GOR can raised to 82.12kgh^{-1} and 5.14,

respectively, once the heat pump subsystem was coupled. Furthermore, the definition of fully coupled system, which announced no extra heater or cooler was need to satisfy the sprayed conditions of the seawater, was proposed, and fully coupled conditions appeared at the designated range of the mass flow rate ratio (MFRR) between the seawater and dry air. Dehghani [21] investigated the performance of the integrated system with the closed-air HD desalination unit with direct contact dehumidifier and a heat pump, which provided the cooling and heating loads simultaneously. After building the mathematical models, the desalination performance of the integrated system at different conditions were focused. It was found that under a fixed salinity of the seawater and freshwater temperatures, the fully coupled conditions of the HD desalination system can be available, by changing the MFRR between the seawater and freshwater or seawater and dry air.

According to the literature survey, it was concluded the heat pump integration into the HD desalination system has been the research focus all over the world, and it is proved to be an effective way to improve the desalination performance. Based on the performance improvement from the combination between the closed-air configurations and heat pump, it can be inferred that there is still potential to enhance the performance of desalination, through recovering the carried water from the discharged air, for the HD desalination configuration with open-air frames [22]. He [23] coupled the heat pump into an open-air HD desalination system, with a plate heat exchanger as dehumidifier. The relations between the critical thermal parameters and performance of desalination were explored. After the optimization with particle swarm algorithm, a top water production as 151.03kgh^{-1}, and gained-output-ratio as 5.95, for the gained-output-ratio, were obtained within the decision variable range. However, it was found that the thermodynamic performance of the open-air desalination system was restricted due to an extra heat load for almost all the involved conditions. Furthermore, the direct contact dehumidifier was proved to be useful, relieving the problems resulting from the surface type condenser, such as suffering corrosion, low heat transfer coefficient and high cost [24, 25], and it has been applied and investigated in the closed-air HD

desalination unit with the heat pump coupled [21]. Therefore, it is a novel idea, taking the concepts of open-air, open-water configuration, packing bed dehumidifier, heat pump together into consideration, which has not been reported, to further explore the energy conservation potential in the heat pump powered HD desalination system, and the thermodynamic performance of such system should also be optimized through the particle swarm algorithm to fill the research gap in the literature.

In this paper, a novel combined system, with a heat pump coupled into the HD desalination system with OAOW configurations, is proposed, in which the packings are used in the dehumidifier. An evaporator is assigned after the dehumidifier, and the freshwater can be obtained both from the dehumidifier and evaporator, with the latent heat of the discharged humid air recovered during condensation. Based on the conservation relations, thermodynamic analysis, at the energetic and entropic viewpoints, are both conducted, to determine the available thermodynamic performance of the HPPDS. Thermodynamic investigation is initially completed to determine the correlations between the prescribed parameters and the system performance, and then the optimization analysis based on PSO algorithm is then introduced to explore the further energy conservation potential of the HPPDS, obtaining the best performance of desalination and the corresponding decision parameters. The research method and results supply a novel enhancement measure aiming to the HD desalination system, and also presents important references for the further design and optimization.

2. Description of the heat pump powered desalination system

The detailed scheme of the HPPDS and relevant energy conversion conditions are described in Fig. 1 and Fig. 2, respectively, with the OAOW humidification dehumidification and heat pump subsystems coupled. In the HD desalination system, the ambient air is humidified by contacting the hot spraying seawater, and then it is condensed under the cooling effect from the spraying cold water in the packed bed dehumidifier. Finally, it is further dehumidified, releasing heat to evaporate the refrigerant cycling in the heat pump. The ambient seawater is first

preheated in the recuperator to recover the internal energy of the discharged water from the dehumidifier, and it is further heated in the condenser, absorbing the latent heat of condensation for the refrigerant. It can be also observed that there is an auxiliary heater or cooler due to the possible imbalance between the released heat of the refrigerant and the heat demand to generate the spraying conditions of the seawater. The hot seawater is sprayed into the packed bed humidifier, concentrated during humidifying the ambient air, and it is finally discharged into the ambient. In the HD desalination system with packed bed dehumidifier, the cold water is applied to condense the hot humid air after humidification, and the condensed water comes into the sprayed cold water together. As a result, the initially sprayed cold water is heated, and the hot discharged water is cooled with the ambient seawater preheated. Finally, the condensed water during dehumidification within the cooled water is obtained as the production, while the remaining water is conducted into the dehumidifier, closing the water cycle.

As demonstrated, the heat pump is used to enhance the energy utilization efficiency of the HD desalination system, and the evaporator is applied to recover the internal energy as well as the carried water of the dehumidified air, while the condenser is used to heat the seawater. Furthermore, the evaporated refrigerant is pressurized during compression in the compressor to form the temperature difference between the refrigerant and seawater, and the valve is used to throttle the high pressure condensate.

It can be summarized that both the condensate from the dehumidifier and evaporator is the water production of the HPPDS, and then the energy conversion efficiency can be improved with the HD desalination and HP coupled.

In order to construct the mathematical models of the HPPDS and complete the performance simulation, the following assumptions are given out:

(1) The HPPDS is operating at the steady state conditions.

(2) Energy loss into the environment, potential and kinetic energy difference during any thermal processes are not taken into account.

(3) Foulings of all the involved heat exchangers are ignored.

(4) Power consumptions of the pumps, blowers are negligible [26].

(5) The states of the refrigerant at the outlets of the condenser and evaporator are saturated.

3. Mathematical models of the HPPDS with OAOW configurations

3.1 Humidifier

In the HPPDS with OAOW configurations, humidifier is one of the core components, in which the inflow air will contact the sprayed seawater direct. In order to raise the contact area during heat and mass transfer, the structured packings are filled in the humidifier, with Sulzer Mellapak 250 Y. During the heat and mass transfer between the ambient air and sprayed seawater, the principles of mass and energy conservation can be illustrated in Eq. (1) and Eq. (2):

$$m_{da}(\omega_2 - \omega_1) = m_{sw} - m_b \tag{1}$$

$$m_{da}(i_{a2} - i_{a1}) = m_{sw} i_{sw,o} - m_b i_b \tag{2}$$

In the HD desalination subsystem, the humidification performance is directly linked to the water producing capacity in the following condensing both in the dehumidifier and evaporator. In view of the unsaturated air from the ambient, the general definition of effectiveness [27] is adopted to characterize the performance of humidification, with the necessary entropic analysis followed to judge the feasibility of the relevant input parameters

$$S_{gen,h} = m_b s_b - m_{sw} s_{sw,o} + m_{da}(s_{a2} - s_{a1}) \tag{3}$$

3.2 Dehumidifier

Obviously, after the humidification, the humidified air will enter the filled packings to contact with the sprayed cold water at the top of the dehumidifier, and it will be condensed. Due to the application of the packings in the dehumidifier, the similar mass and energy conservation equations can be gained as follows:

$$m_{w,d} = m_{w1} - m_{w0} = m_{da}(\omega_2 - \omega_3) \tag{4}$$

$$m_{w1} i_{w1} - m_{w0} i_{w0} = m_{da}(i_{a2} - i_{a3}) \tag{5}$$

During the dehumidification , the general definition of energy effectiveness is also adopted to illustrate the corresponding heat and mass transfer performance. However, it was proved that the temperature pinch will always emerge at the terminal due to the temperature relations between the hot air and the cold water [16]. Hence, the entropy generation rate during dehumidification, $S_{gen,d}$, can be calculated to illustrate the process irreversible loss.

$$S_{gen,d} = m_{w1} s_{w1} - m_{w0} s_{w0} + m_{da}(s_{a3} - s_{a2}) \tag{6}$$

3.3 Recuperator

After the dehumidification, the condensed water and the sprayed water merge, and the cold water is also heated during the latent heat releasing for the humid air. Consequently, the internal energy of the discharged water should be recovered to raise the energy utilization efficiency of the entire HPPDS, with a recuperator to preheat the inflow seawater. The conservation equations both considering the energetic and entropic aspects are given out.

$$Q_{re} = m_{sw}(i_{sw,i} - i_0) = m_{w1}(i_{w1} - i_{w0}) \tag{7}$$

$$S_{gen,re} = m_{sw}(s_{sw,i} - s_0) + m_{w0} s_{w0} - m_{w1} s_{w1} \tag{8}$$

3.4 Condenser

As the enhancement method, a heat pump is coupled into the general HD desalination subsystem. Thereinto, the condenser from the heat pump is used to achieve the energy input, powering the HD desalination unit, and then the seawater is prepared to be sprayed into the filled packings. Within the condenser, the heat transfer rate can be acquired as:

$$Q_{con} = m_{sw}(i_{sw,m} - i_{sw,i}) = m_r(i_{con,i} - i_{con,o}) \tag{9}$$

In the heat pump, the refrigerant absorbs the internal energy from the humid air in the evaporator, and it is pressurized during compression. However, when the refrigerant is condensed to the saturated liquid in the

condenser, the corresponding released heat can not always balance the energy demand to prepare the sprayed seawater into the filled packings of the humidifier. Thus, an auxiliary heat exchanger as a heater or cooler must be prepared to compensate the energy difference, and the corresponding heat transfer rate can be obtained as:

$$\begin{cases} Q_h = m_{sw}(i_{sw,o} - i_{\mathrm{sw,m}}) \\ Q_c = m_{sw}(i_{sw,m} - i_{\mathrm{sw,o}}) \end{cases} \tag{10}$$

For the respect of entropic analysis, the equivalent entropy generation rate during condensation plus the heating or cooling can be expressed as:

$$S_{gen,con} = m_{sw}(s_{sw,o} - s_{sw,i}) + \frac{m_{sw}(i_{sw,o} - i_{sw,i})}{i_{con,i} - i_{con,o}}(s_{con,o} - s_{con,i}) \tag{11}$$

3.5 Throttle valve

After the condensation, the refrigerant must be throttled in the valve to evaporate at a lower pressure, and the energetic and entropic balance can be illustrated as:

$$i_{e,i} = i_{con,o} \tag{12}$$

$$S_{gen,v} = m_r(s_{e,i} - s_{con,o}) \tag{13}$$

3.6 Evaporator

In the general open-air, open-water HD desalination subsystem, the dehumidified air is induced into the environment directly. Actually, there is still potential to recover the internal energy of the discharged air and reduce the humidity ratio, and thus both the water production and energy utilization efficiency can be elevated. As a result, the evaporator is applied to cool the humid air, with the refrigerant absorbing the released energy.

$$m_{w,\mathrm{e}} = m_{da}(\omega_3 - \omega_{3,o}) \tag{14}$$

$$Q_e = m_r(i_{e,o} - i_{e,i}) = m_{da}(i_{a3} - i_{a3,o}) - m_{w,e}i_{w,e} \tag{15}$$

$$S_{gen,e} = m_r(s_{e,o} - s_{e,i}) + m_{da}(s_{a3,o} - s_{a3}) + m_{w,e}s_{w,e} \tag{16}$$

3.7 Compression

After the refrigerant evaporates, it is pressurized during compression to prepare for heating the preheated seawater from the recuperator, and the corresponding conservation equations are given out as follows, with a compression efficiency of η_c=0.8.

$$W_c = m_r(i_{con,i,s} - i_{e,o})/\eta_c \tag{17}$$

$$S_{gen,c} = m_r(s_{con,i} - s_{e,o}) \tag{18}$$

3.8 Evaluation of the HPPDS

For the integrated heat pump, coefficient of performance (COP) can be applied to evaluate the relevant thermal efficiency, calculated by Eq. (17).

$$COP = \frac{Q_{con}}{W_c} \tag{19}$$

For the entire HPPDS, the gained-output-ratio can be used to assess the overall energy conversion efficiency, in which the system profit is mainly attributed to the water production during dehumidification and evaporation, while the energy input comes from the released heat during the refrigerant condensation and heating process in the auxiliary heat exchanger.

$$\begin{cases} GOR = \dfrac{m_{w,d} i_{fg,d} + m_{w,e} i_{fg,e}}{W_c + Q_h} & Q_h > 0 \\ GOR = \dfrac{m_{w,d} i_{fg,d} + m_{w,e} i_{fg,e}}{W_c} & Q_c \geq 0 \end{cases} \tag{20}$$

In addition of the energetic aspect, the entropic analysis of the entire HPPDS can also be achieved, analyzing the distribution of the irreversible loss.

$$\begin{cases} S_{gen,t} = S_{gen,h} + S_{gen,d} + S_{gen,\mathrm{re}} + S_{gen,con} + S_{gen,v} + S_{gen,e} + S_{gen,c} \\ s_{gen,t} = \dfrac{S_{gen,t}}{m_{w,d} + m_{w,e}} \end{cases} \tag{21}$$

After modeling the entire HPPDS with OAOW configurations, the performance simulation and optimization can be completed through the Matlab platform.

4. Validation of the HPPDS with OAOW configurations

For the current HPPDS, with the heat pump and HD desalination subsystems coupled, the performance of the core humidification and dehumidification is verified with the published results from Narayan [28], and the relevant comparison results [22] can be inherited to validate the current model. A maximum deviation of the heat capacity ratio during humidification, HCR_h, is found with a value of 4.2%, with which the model accuracy of the entire system is proved.

5. Results and discussion

According to the established mathematical models for the open-air, open-water HPPDS, the thermodynamic analysis, both at the energetic and entropic aspects, is first attained under the design conditions in Table 1. It is found that the pinch temperature difference for the condenser, PTD_{con}, and terminal temperature difference for the evaporator, TTD_e, are assumed at 10K. The general effectiveness of humidification and dehumidification stays at ε=0.85, while the terminal temperature difference for the recuperator is assumed at TTD_{re}=5K. Moreover, for the heat pump, the design pressure ratio during compression is fixed at PR=4.

5.1 Thermodynamic analysis of the HPPDS at design conditions

A. Entropic aspect

As stated previously, the general energy effectiveness is conducted to characterize the performance during humidity-varied process. However, due to the defects with an intermediate zero pinch without a temperature cross [16], which will locate in the unfeasible regions for the thermal parameters, the entropic analysis to calculate the specific entropy generation rate should be first completed. Therefore, the corresponding calculation results of all the specific entropy generation rates are achieved and presented in Fig. 3.

It is calculated that all the specific entropy generation rates except the value of humidification are positive, which means the corresponding processes are possible to be achieved at the prescribed input conditions. However,

with respect to the humidification, it can be obtained that unfeasible regions from MFRR=1.6 to MFRR=2.4 are existing at the assumption of ε_h=0.85, and the minimum value of specific entropic generation rate, $s_{gen,h}$, approaches $s_{gen,h}$=-0.07kJkg^{-1}K^{-1}, at the balance condition during humidification, with the heat capacity ratio as HCR_h=1. By accumulating the specific entropy generation rate, it can be gained that the bottom entropy generation rate arrives at $s_{gen,t}$=0.68Jkg^{-1}K^{-1}. However, due to the existing of the unfeasible regions, the actual bottom specific entropy generation rate for the entire HPPDS is $s_{gen,t}$=0.84Jkg^{-1}K^{-1} at *MFRR*=1.6, which is also a quantitative index to measure the energy utilization efficiency of the HPPDS.

B. Energetic aspect

After eliminating the impossible conditions on the basis of the entropic analysis, the actual HPPDS performance can be acquired through energetic investigation. Water production, both from dehumidification and condensation in the evaporator is calculated, shown in Fig. 4. Evidently, in the HD desalination systems, water production comes from the cycling dry air involved and the variation of the humidity ratio. For the produced water during dehumidification, it can be seen in Fig. 4 that the difference of humidity ratio increases from $\Delta\omega_d$=30.23gkg^{-1} at *MFRR*=1 to $\Delta\omega_d$=112.71gkg^{-1} at *MFRR*=5, while the relevant mass flow rate of the cycling dry air drops from m_{da}=0.5kgs^{-1} to m_{da}=0.1kgs^{-1}. In view of the completely reverse trends of the air mass flow rate and humidity ratio difference, the maximum water production during dehumidification reaches $m_{w,d}$=79.36kgh^{-1}, while the actual relevant value is $m_{w,d}$=74.08kgh^{-1} at *MFRR*=1.6. Furthermore, to explore the potential of the water production as well as the energy utilization efficiency, an evaporator within the heat pump subsystem is applied to condense the discharged humid air after dehumidification, and the actual water production in the evaporator is found as $m_{w,e}$=15.18kgh^{-1} at *MFRR*=1.6. Actually, the relevant temperature and humidity ratio of the discharged humid air after dehumidification are T_{a3}=303.75K and ω_3=28.20gkg^{-1}, while the ambient temperature and humidity ratio are T_{a3}=288.15K and ω_1=5.28gkg^{-1}, respectively. Finally, taking the water production both from the

dehumidification and condensation in the evaporator, a total value of the actual water production as m_w=89.27kgh^{-1} is obtained.

Thermal efficiency is another quota to characterize the desalination performance. Obviously, it is expectable that the energy conversion can be improved, because energy recovery is enhanced once the heat pump subsystem is involved. The energy distribution within the entire HPPDS is calculated and presented in Fig. 5. In the light of the assumptions with PR=4, PTD_{con}=TTD_e=10 and the saturated state at the outlets of the evaporator and condenser, it is certain that the specific enthalpy variations for the heat pump keep the same, although the cycling mass flow rate of the refrigerant will vary with the MFRR between the seawater and humid air. As a result, based on the definition of COP, the relevant value keeps at COP=3.83. Actually, the variation trend of the heat transfer rate within the evaporator is consistent with that of the relevant water production, shown in Fig. 4, because the latent heat during condensation of the humid air is the dominant part of the total heat transfer rate. Consequently, the mass flow rate of the cycling refrigerant and power consumption decrease from m_r=0.21kgs^{-1} and W_c=9.29kW to m_r=0.04kgs^{-1} and W_c=1.95kW at the prescribed range of the MFRR. Furthermore, for the current configurations, an auxiliary heat exchanger, regarded as a heater or cooler lying on the comparison between the energy supply from the refrigerant in the condenser and the energy demand of the sprayed seawater during humidification. It can be discovered that the heat load of such an auxiliary heat exchanger is always positive, which represents that a heater is available to raise the temperature of the seawater from the condenser. As a result, the energy input into the HPPDS are determined from the accumulation both of the power consumption during compression and the heater heat load. Taken the water production and total energy input into account, a peak value of the actual energy conversion efficiency as GOR=4.17 is obtained, when the mass flow rate ratio locates at $MFRR$=1.6.

5.2 Parametric analysis of the HPPDS: HD desalination system

A. Humidification effectiveness

In addition of the performance investigation at the design conditions, the parametric analysis of the HPPDS is also conducted to explore the influence extent from the critical states. The humidification effectiveness is first selected as the objective variable to complete the parametric analysis, and the relevant results are calculated and exhibited in Fig. 6. It is seen that the humidification performance is very critical for the desalination performance, the top value of the actual water production is raised to m_w=93.80kgh^{-1} at *MFRR*=1.4 from m_w=85.02kgh^{-1} at *MFRR*=1.8, when the humidification effectiveness rises from ε_h=0.8 to ε_h=0.9. Such variation of the water production can be explained through the temperature change of the humid air in response to the effectiveness alternation. In fact, a higher effectiveness announces a smaller terminal temperature difference at the outlet of the humidifier, when the other conditions keep the same. Therefore, the temperature as well as the humidity ratio of the humid air after humidification will rise once the effectiveness increases. Taking the case of *MFRR*=1.4 for instance, the humidified temperature arrives at T_{a2}=323.42K at ε_h=0.9, while the original value is T_{a2}=321.51K at ε_h=0.8. Based on the humidity ratio difference between the air after humidification and the discharged air to the ambient, the water production can be promoted evidently.

The variation of the effectiveness will change the characteristics of the humidification obviously. However, the change of the energy demand of the sprayed seawater is not sensitive to the effectiveness alternation, with a decrease difference of 4.73kW from ε_h=0.8 to ε_h=0.9 at the case of *MFRR*=1.4. On the other hand, the temperature of the discharged air from dehumidification will also rise because the dehumidification effectiveness keeps the same, while the air temperature of the humid air is raised. As a result, the mass flow rate of the cycling refrigerant increases, and the corresponding compression power and the heat load of the evaporator and condenser is elevated to W_c=7.14kW, Q_e=20.18kW and Q_{con}=27.32kW at the case of *MFRR*=1.4 and ε_h=0.9, while the relevant values are W_c=5.36kW, Q_e=15.16kW and Q_{con}=20.52kW at the case of *MFRR*=1.4 and ε_h=0.8. Considering all the values of the heat load and compression power, it is concluded that the total energy input will actually drops a lot from

20.70kW to 10.95kW at the case of *MFRR*=1.4, when the humidification rises from ε_h=0.8 to ε_h=0.9. Based on the water production elevation and the reduced energy input in response, the top value of the actual GOR is raised from *GOR*=3.14 at ε_h=0.8 to *GOR*=5.74 at ε_h=0.9. The best desalination performance and relevant conditions at different prescribed effectiveness during humidification are listed in Table 2

B. Dehumidification effectiveness

Different values of dehumidification effectiveness, with ε_d=0.8, 0.85 and 0.9 are also designated to conduct the parametric analysis, and the relevant results are presented in Fig. 7. It can be summarized that the HPPDS performance is not sensitive to the characteristics of dehumidification at all. It is discovered that the top water production will be slightly influenced after the effectiveness rises, from m_w=90.20kgh^{-1} at ε_d=0.8 to m_w=88.35kgh^{-1} at ε_d=0.9. Such slight decrease of the water production after the elevation for the dehumidification effectiveness is also well explained. Actually, the elevation of the effectiveness declares the performance improvement during dehumidification, and the relevant water production is raised from $m_{w,d}$=70.47kgh^{-1} at ε_d=0.8 to $m_{w,d}$=77.56kgh^{-1} at ε_d=0.9. However, the elevation of the effectiveness also results in the temperature declination of the discharged air from the dehumidifier. As a result, the case with a higher dehumidification effectiveness will reduce the water production from the evaporator, from $m_{w,e}$=19.73kgh^{-1} at ε_d=0.8 to $m_{w,e}$=10.79kgh^{-1} at ε_d=0.9. Finally, the total water production is slightly influenced negatively, when the effectiveness during dehumidification rises, shown in Table 3.

As stated previously, the elevation of the effectiveness will contribute to the temperature declination of the discharged air out of the dehumidifier. The following result is that the heat load both of the evaporator and condenser, the compression power will decrease due to the mass flow rate declination for the cycling refrigerant. On the other hand, the elevation of the dehumidification effectiveness will also contribute to a higher temperature of the discharged water from the dehumidifier, which indicates that the energy demand of the sprayed conditions of

the seawater will be decreased a lot, from 32.10kW at ε_d=0.8 to 24.12kW at ε_d=0.9. In combination with the compression power and the heat load of the auxiliary heater, the total energy input have a very limited decrease from 14.52kW at ε_d=0.8 to 14.15kW at ε_d=0.9. Finally, a limited elevation for the GOR, from *GOR*=4.16kW at ε_d=0.8 to *GOR*=4.18 at ε_d=0.9, is obtained.

C. Inlet humidity

The open-air, open-water configurations are applied in the current HPPDS. Therefore, the alternation of the air inlet humidity indicates the change of the wet bulb temperature although the dry bulb temperature keeps the same. As a result, the characteristics of the humidification as well as the entire desalination system will response to the humidity alternation. Different inlet humidity, with φ_{a1}=0.3, 0.5 and 0.7 are appointed to reveal the relation between the humidity and the desalination performance, presented in Fig. 8. It can be seen that the top water production will benefit from a lower inlet humidity, with m_w=87.61kgh^{-1} at φ_{a1}=0.7 to m_w=91.62kgh^{-1} at φ_{a1}=0.3. The positive effect can be well explained from the mass transfer process. Actually, a lower inlet humidity announces that the difference between the saturated pressure of the sprayed seawater and the steam partial pressure of the ambient air rises, and the relevant mass transfer process during humidification is enhanced especially at the bottom. Hence, it is obtained that both the temperature and humidity ratio are elevated, with T_{a2}=324.31K and ω_2=60.74gkg^{-1} at φ_{a1}=0.7 to T_{a2}=325.15K and ω_2=96.14gkg^{-1} at φ_{a1}=0.3, when the value of MFRR keeps at *MFRR*=1.6. Based on the same discharged temperature and humidity according to the assumptions, the total water production will obviously promoted for the low ambient humidity case. Actually, the produced water during dehumidification and evaporation is raised from $m_{w,d}$=73.03kgh^{-1} and $m_{w,e}$=14.16kgh^{-1} at φ_{a1}=0.7 to $m_{w,d}$=75.25kgh^{-1} and $m_{w,e}$=16.37kgh^{-1} at φ_{a1}==0.3, when the MRFF stays at *MFRR*=1.6, shown in Table 4.

With a higher temperature and humidity at low ambient humidity, the temperature of the dehumidified air is also raised. Based on the heat balance in the evaporator, the refrigerant mass flow rate will also rise, and then the

compression power is raised from W_c=4.56kW at φ_{a1}=0.7 to W_c=5.22kW at φ_{a1}=0.3. However, the relevant change laws of the necessary compensation energy from the auxiliary heater is different. It is obtained that the auxiliary energy, as the heat load difference between the refrigerant and sprayed seawater, is elevated from 11.53kW at φ_{a1}=0.7 to 7.13kW at φ_{a1}=0.3. Considering the water production, compression power and auxiliary energy from the heater, it is calculated that the top thermal efficiency of the HPPDS is improved from *GOR*=3.79 at φ_{a1}=0.7 to *GOR*=4.96 at φ_{a1}=0.3, shown in Table 4.

5.3 Parametric analysis of the HPPDS: Heat pump

A. pressure ratio

The influence investigation focuses on the performance correlations between the HD desalination subsystem and the entire HPPDS. However, the characteristic parameters of the heat pump subsystem are also important for the system performance. In the HPPDS, the compressor is one of the power sources to drive the HD desalination unit, and the relevant characteristics are important for the system performance. The compression pressure ratio, PR, is prescribed as the first parameter, and the corresponding influence principle is simulated and presented in Fig. 9, without the impossible conditions. As presented in Table 1 for the fixed values of TTD_e, with TTD_e=10K, and $T_{a3,o}$ with $T_{a3,o}$=293.15K, the evaporation temperature and dependent pressure of the refrigerant keep at $T_{e,i}$=$T_{e,o}$=283.15K. As a result, once the pressure ratio of compression rises, the refrigerant temperature at the outlet of the compressor and the relevant condensing temperature will rise significantly. Moreover, under the fixed values of PTD_{con} with PTD_{con}=10K and humidification effectiveness of ε_h=0.85, the sprayed temperature of seawater, $T_{sw,o}$, and the air temperature after humidification will also rise. Taking the condition of *MFRR*=1.4 for instance, which has the maximum actual water production and GOR under the compression pressure ratio of *PR*=3.5, the corresponding sprayed temperature of seawater and air temperature after humidification are promoted from $T_{sw,o}$=324.38K and T_{a2}=319.48K at *PR*=3.5 to $T_{sw,o}$=339.61K and T_{a2}=325.06K at *PR*=4.5. Obviousyly, regardless

of the distribution of water production between the dehumidification and evaporation, a higher air temperature at the humidifier outlet also announces a higher total water production owing to the same temperature of the final discharged air to the ambient. Finally, it can be seen that the total peak water production arrives at m_w=106.53kgh^{-1}, with $m_{w,d}$=87.01kgh^{-1} and $m_{w,e}$=19.52kgh^{-1}, at PR=4.5 from m_w=71.29kgh^{-1}, with $m_{w,d}$=59.77kgh^{-1} and $m_{w,e}$=11.52kgh^{-1}, at PR=3.5, presented in Table 5.

As illustrated previously, the temperature of the humidified air is raised significantly after the elevation of the compressor pressure ratio. Therefore, the relevant temperature of the discharged air after dehumidification will also rise at a constant effectiveness of dehumidification as ε_d=0.85. Due to an almost fixed value for the specific enthalpy difference of the refrigerant during evaporation, the cycling refrigerant mass flow rate and the compression power consumption will increase after the pressure ratio elevation. Also taking the case of $MFRR$=1.4 for example, the compression power rises from W_c=3.16kW at PR=3.5 to W_c=10.48kW at PR=4.5. On the other hand, due to the sprayed temperature elevation of the seawater, the corresponding energy demand is also raised from 23.90kW to 43.60kW at the case of $MFRR$=1.4, while it mainly results from the increase of the heat transfer rate during evaporation from Q_e=10.68kW at PR=3.5 to Q_e=25.22kW at PR=4.5. As a result, the auxiliary heat demand is reversely reduced from Q_h=10.07kW at PR=3.5 to Q_h=7.90kW at PR=4.5. Based on the redistribution of the energy conversion after the pressure ratio elevation, it can be concluded that the thermal efficiency of the desalination system is really improved. The top value of the actual GOR reaches GOR=4.54 at PR=4.5 with the variation trends of the water production, heat demand of the sprayed seawater, the compression power and the auxiliary heat load taken into account.

B. PTD of the condenser

Obviously, the PTD of the condenser is related to the temperature of the sprayed seawater directly, and the relevant alternation will change the production and thermal efficiency of the HPPDS. Thus, the parametric analysis

from different values of the PTD_{con} with PTD_{con}=5K, 10K, 15K, is also conducted and presented in Fig. 10. It is very obvious that a lower value of PTD_{con} announces a higher water production and relevant desalination efficiency. Actually, the influence mechanism from the alternation of the PTD_{con} is similar with that from the pressure ratio variation. Once the value of PTD_{con} is reduced, the temperatures of the sprayed seawater, the condensing refrigerant and humid air before and after dehumidification will be raised together, and the actual peak water production is raised from m_w=75.42kgh^{-1} at PTD_{con}=15K, with $m_{w,d}$=62.02kgh^{-1} and $m_{w,e}$=13.40kgh^{-1}, to m_w=103.12kgh^{-1} at PTD_{con}=5K, with $m_{w,d}$=85.44kgh^{-1} and $m_{w,e}$=17.68kgh^{-1}, shown in Table 6.

With respect to the energy conversion, the variation of the energy input should also be considered after the alternation of the PTD_{con}. For example, the maximum water production and desalination efficiency can be found at the case of *MFRR*=1.4, with m_w=75.42kgh^{-1} and *GOR*=3.65, when the value of PTD_{con} stays at PTD_{con}=15K, and the relevant energy demand to form the sprayed conditions increases from 26.19kW to 41.18kW at PTD_{con}=5K. Thereinto, the effective energy input, Q_h, which is transferred into the seawater through the heater, is almost the same after the PTD_{con} alternation, because the elevation magnitudes reaches ΔW_c=3.92kW for the compression power and ΔQ_e=11.07kW for the heat load of the evaporator. Finally, based on the variation trends of the energy input from all the involved devices, a promotion of the top GOR as 24.66%, from *GOR*=3.65 at PTD_{con}=15K to *GOR*=4.55 at PTD_{con}=5K is verified.

C. TTD of the evaporator

Different values of TTD during evaporation, with TTD_e=5K, 10K, 15K, are also appointed to achieve the parametric analysis, investigating the relevant influence principles shown in Fig. 11. It is evident that once the value of TTD_e is reduced, the inlet temperature as well as the pressure of the refrigerant into the compressor will rise. As a result, all the temperatures of the outlet refrigerant for the compressor, the sprayed seawater, the humid air before and after dehumidification will be raised significantly. As the influence mechanisms between the

involved temperatures and the water production and GOR, it is found that the elevation of the top water production, m_w, approaches Δm_w=40.85kgh^{-1}, from m_w=69.40kgh^{-1} at TTD_e=15K, with $m_{w,d}$=58.72kgh^{-1} and $m_{w,e}$=10.68kgh^{-1}, to m_w=110.25kgh^{-1} at TTD_e=5K, with $m_{w,d}$=88.67kgh^{-1} and $m_{w,e}$=21.58kgh^{-1}, shown in Table 7. Furthermore, due to the significant elevation of the water production with Δm_w=40.85kgh^{-1}, and the relatively limited increase for the total energy input with 3.27kW, the thermal efficiency of the HPPDS is improved, from *GOR*=3.60 at TTD_e=15K to *GOR*=4.54 at TTD_e=5K. The best desalination performance and relevant conditions at different TTD_e are also listed in Table 7.

5.4 Optimization of desalination performance

After the parametric analysis, the influence laws from the prescribed parameters on the performance of the HPPDS is obtained. However, the overall influence from all the parameters should also be investigated to find the relevant conditions, having the best desalination performance. Therefore, the algorithm of particle swarm optimization (PSO) [29] is applied to conduct the thermodynamic optimization aiming to the HPPDS. During the optimization, the particle number and iterations, represented by N and M, are fixed as *N*=50 and *M*=100, respectively, while the location, X, and velocity, V, can be updated according to Eq. (22), with the constants and coefficients in Table 8:

$$\begin{cases} X_{id}^{k+1} = X_{id}^{k} + V_{id}^{k+1} \\ V_{id}^{k+1} = \omega \times V_{id}^{k} + c_1 \times rand_1^{k} \times (Pbest_{id}^{k+1} - X_{id}^{k}) + c_2 \times rand_2^{k} \times (Gbest_{id}^{k+1} - X_{id}^{k}) \end{cases} \tag{22}$$

The current optimization belong to the single objective pattern, and the relevant location vector, X, contains the ratio between the mass flow rate of the seawater and humid air, MFRR, humidification and dehumidification effectiveness, ε_h and ε_d, pressure ratio of the compressor, PR, pinch temperature difference for the condenser, PTD_{con}, and terminal temperature difference for the evaporator, TTD_e, while GOR is regarded as the objective function. Hence, the optimization objective can be expressed as the function of the decision variables in Eq. (23), with the corresponding lower and upper limits in Table 9:

$$\begin{cases} \min GOR = f(X) = f(MFRR, \varepsilon_h, \varepsilon_d, \mathrm{PR}, PTD_{con}, TTD_e) \\ S_{gen,h}(X) \geq 0 \\ LL \leq X \leq UL \end{cases} \tag{23}$$

Finishing the thermodynamic optimization, the best desalination performance of the HPPDS under the appointed range of the decision variables are acquired and presented in Table 10. It is gained the actual peak water production approaches m_w=150.75kgh^{-1}, with $m_{w,d}$=118.84kgh^{-1} during dehumidification and $m_{w,e}$=31.92kgh^{-1} during evaporation in the evaporator. On the basis of the water production, m_w=150.75kgh^{-1}, and the total energy input, with W_c=12.28kW and Q_h=0.02kW, the maximum value of GOR arrives at GOR=8.12. Furthermore, in view of the monotonic relations between the variables and desalination performance from the parametric analysis, the optimized values for the decision variables are found at MFRR=2.17, ε_h=ε_d=0.9, PR=4.5, PTD_{con}=5K and TTD_e=5K.

From the optimization results, it is concluded that the desalination performance is very excellent with the water production as m_w=150.75kgh^{-1} and GOR as GOR=8.12. Furthermore, it is also found that such a HPPDS with the optimized parameters can almost avoid the application of the auxiliary heater, with Q_h=0.02kW, which can be called the fully coupled HPPDS between the HD desalination and heat pump subsystems.

The performance comparison between the current HPPDS and our previous research [23] is also given out in Table 10. It is obvious that the difference of water production both from the dehumidifier and evaporator is very limited, with a value of Δm_w=0.27kgh^{-1}. However, the running conditions of the heat pump are different, and the result is that an extra heat load is available to raise the spraying temperature of seawater into the humidifier, Q_h=6.29kW, for the desalination system with a plate heat exchanger as dehumidifier, while the current system with a direct contact dehumidifier is fully coupled. Finally, a top value of GOR reaches 8.12 for the fully coupled system, while it is only 5.95 for the surface dehumidifier desalination system [23].

6. Conclusions and future work

In this paper, the advantages of energy conservation are proved, after a heat pump is conducted into a open-air, open-water HD desalination system. After the thermodynamic analysis and optimization through PSO algorithm, the conclusions from the calculation results are given out as follows:

1. In combination with the energetic and entropic analysis into consideration, the best desalination performance of the proposed HPPDS is found when the value of MFRR stays at 1.6. The peak water production approaches 89.27kgh^{-1}, with 74.08kgh-1 during dehumidification and 15.18kgh^{-1} from the refrigerant condensation in the evaporator. With the energy input both from the power consumption of compression and heat load of the auxiliary heater, a top efficiency of 4.17 is achieved.

2. The desalination performance of the HPPDS is very sensitive to the humidification effectiveness. The top water production will rise from 85.02kgh^{-1} to 93.80kgh^{-1}, when the humidification effectiveness is elevated from 0.8 to 0.9. In combination with the relevant decrease trend for the energy input in response to the effectiveness elevation, the value of GOR is raised significantly to 5.74, when the humidification effectiveness locates at 0.9.

3. The influence from the dehumidification on the desalination performance of the HPPDS is very limited. The water production is reduced slightly, with a magnitude of 1.85kgh^{-1}, when the effectiveness during dehumidification rises from 0.8 to 0.9, while the relevant value of GOR is reversely changed from 4.16 to 4.18.

4. Due to a lower wet bulb temperature due once the ambient humidity decreases, the top water production and GOR are improved to 91.62kgh^{-1} and 4.96, when the ambient humidity reaches 0.3, which mainly attributed to the mass transfer enhancement during humidification.

5. A higher pressure ratio of compression and lower PTD_{con} and TTD_e are benefit to improve the system water production and GOR. Furthermore, it is found that the relevant influence mechanisms with such improvements are consistent.

6. After the thermodynamic optimization, the maximum water production and GOR can arrive at 150.75kgh^{-1}

and 8.12, respectively. It is also found that the desalination system with the optimized performance arrives at the fully coupled conditions, in which the auxiliary heater is not available to compensate the energy input.

7. According to the comparison of desalination performance between the current and the previous configurations, it is found that the HPPDS with a direct contact dehumidifier has obvious advantages at the aspect of energy conservation, compared with the system with a surface dehumidifier.

In addition of the thermodynamic analysis, the economic aspect should also be considered to explore the potential of actual application. Consequently, multi-objective optimization will be available to well balance the thermodynamic and economic performance.

Acknowledgements

The authors gratefully acknowledge the financial support by the National Natural Science Foundation of China (Grant No. 51406081), the Hong Kong Scholars Program (Grant No. XJ2017040) and The Hong Kong Polytechnic University, the Fundamental Research Funds for the Central Universities (NO.NP2018107).

References

[1] R. Tariq, N.A. Sheikh, J. Xamán, A. Bassam. An innovative air saturator for humidification dehumidification desalination application. Applied Energy, 228 (2018): 789-807.

[2] N.K. Nawayseh, M.M. Farid, S. Al-Hallaj, A.R. Al-Timimi. Solar desalination based on humidification process-I: Evaluating the heat and mass transfer coefficients. Energy Conversion and Management, 40 (1999): 1423-1439.

[3] N.K. Nawayseh, M.M. Farid, A.A. Omar, A. Sabirin. Solar desalination based on humidification process-I: Computer simulation. Energy Conversion and Management, 40 (1999): 1441-1461.

[4] M. Farid, A.W. Al-Hajaj. Solar desalination with a humidification dehumidification cycle. Desalination, 106 (1996): 427-429.

[5] G.P Li, L.Z Zhang. Investigation of a solar energy driven and hollow fiber membrane-based humidification dehumidification desalination system. Applied Energy, 177 (2016): 393-408.

[6] N. Ghaffour, S. Lattemann, T. Missimer, K.C. Ng, S. Sinha. Renewable energy-driven innovative energy-efficient desalination technologies. Applied Energy, 136 (2014): 1155-1165.

[7] A.E. Kabeel, M. Abdelgaied. Experimental evaluation of a two-stage indirect solar dryer with reheating coupled with humidification dehumidification desalination system for remote areas, Desalination, 425 (2018) 22-29.

[8] E.Z. Mahdizade, M. Ameri. Thermodynamic investigation of a semi-open air, humidification dehumidification desalination system using air and water heaters. Desalination, 482 (2018): 182-198.

[9] B.L.D.O. Campos, A.O.S.D. Costa, E.F.D.C. Junior. Mathematical modeling and sensibility analysis of a solar humidification dehumidification desalination system considering saturated air. Solar Energy, 157 (2017): 321-327.

[10] G.P. Narayan, M.H. Sharqawy, J.H. Lienhard, S.M. Zubair. Thermodynamic analysis of humidification dehumidification desalination cycles. Desalination and Water Treatment, 16 (2010): 339-353.

[11] Y. Ghalavand, M.S. Hatamipour, A. Rahimi. Humidification compression desalination. Desalination, 341 (2014): 120-125.

[12] O.K. Siddiqui, M.H. Sharqawy, M.A. Antar, S.M. Zubair. Performance evaluation of variable pressure humidification dehumidification systems. Desalination, 409 (2017): 171-182.

[13] Z. Rahimi-Ahar, M.S. Hatamipour, Y. Ghalavand. Solar assisted modified variable pressure humidification dehumidification desalination system. Energy Conversion and Management, 162 (2018): 321-330.

[14] G.P. Narayan, K.M. Chehayeb, R.K. McGovern, G.P. Thiel, S.M. Zubair, J.H. Lienhard V. Thermodynamic balancing of the humidification dehumidification desalination system by mass extraction and injection. International Journal of Heat and Mass Transfer, 57 (2013): 756-770.

[15] R.K. McGovern, G.P. Thiel, G.P. Narayan, S.M. Zubair, J.H. Lienhard V. Performance limits of zero and single extraction humidification dehumidification desalination systems. Applied Energy, 102 (2013): 1081-1090.

[16] K.M. Chehayeb. Numerical fixed-effectiveness and fixed-area models of the humidification dehumidification desalination system with air extractions and injections. Master's thesis, Massachusetts Institute of Technology, 2014.

[17] X.D. Zhen. Refrigeration Principle and devices. Beijing, Mechanical Industry Press, 2001.

[18] M.B. Shafii, H. Jafargholi, M. Faegh. Experimental investigation of heat recovery in a humidification dehumidification desalination system via a heat pump. Desalination, 437 (2018): 81-88.

[19] Y. Zhang, C.G. Zhu, H. Zhang, W.D. Zheng, S.J. You, Y.H. Zhen. Experimental study of a humidification dehumidification desalination system with heat pump unit. Desalination, 442 (2018): 108-117.

[20] S. Dehghani, A. Date, A. Akbarzadeh. Performance analysis of a heat pump driven humidification dehumidification desalination system. Desalination, 445 (2018): 95-104.

[21] W.F. He, D. Han, C. Ji. Investigation on humidification dehumidification desalination system coupled with heat pump. Desalination, 436 (2018): 152-160.

[22] W.F. He, L. Huang, J.R. Xia, W.P. Zhu, Y.K. Wu. Parametric analysis of a humidification dehumidification desalination system using a direct-contact dehumidifier, International Journal of Thermal Sciences, 120 (2017): 31-40.

[23] W. F. He, J. J. Chen, M. R. Zhen, D. Han. Thermodynamic, economic analysis and optimization of a heat pump driven desalination system with open-air humidification dehumidification configuration. Energy, 174

(2019): 768-778.

[24] T. Rajaseenivasan, K. Srithar. An investigation into a laboratory scale bubble column humidification dehumidification desalination system powered by biomass energy. Energy Conversion and Management, 139 (2017): 232-244.

[25] G.P. Narayan, M.H. Sharqawy, E.K. Summers, J.H. Lienhard, S.M. Zubair, M.A. Antar. The potential of solar-driven humidification-dehumidification desalination for small-scale decentralized water production. Renewable and Sustainable Energy Reviews. 14 (2010): 1187-1201.

[26] W.F. He, F. Wu, T. Wen, Y.P. Kong, D. Han. Cost analysis of a humidification dehumidification desalination system with a packed bed dehumidifier, Energy Conversion and Management, 171 (2018): 452-460.

[27] G.P. Narayan, K.H. Mistry, M.H. Sharqawy, S.M. Zubair, J.H. Lienhard, Energy effectiveness of simultaneous heat and mass exchange devices. Frontiers in Heat Mass Transfer, 023001 (2010): 1-13.

[28] G.P. Narayan, J.H. Lienhard, S.M. Zubair. Entropy generation minimization of combined heat and mass transfer devices. International Journal of Thermal Sciences, 49 (2010): 2057-2066.

[29] J. Kennedy, R. Eberhart. Particle swarm optimization: Neural Networks, 1995.

[30] **Table 1** Design thermodynamic conditions of the HPPDS with OAOW configurations

S (g/kg)	$m_{sw}=m_{w0}$ (kgs^{-1})	$\varepsilon_{h,d}$	φ_{a1}	$\varphi_{a2}=\varphi_{a3}$	PR	$T_{sw,0}=T_{a1}$ (K)	$T_{a3,o}$ (K)	TTD_e (K)	PTD_{con} (K)	TTD_{re} (K)
35	0.5	0.85	0.5	1	4	288.15	293.15	10	10	5

Table 2 Top desalination performance of the HPPDS at different humidification effectiveness

ε_h	$MFRR$	$m_{w,d}$ (kgh^{-1})	$m_{w,e}$ (kgh^{-1})	COP	W_c (kW)	Q_e(kW)	Q_h (kW)	GOR
0.8	1.8	73.79	11.23	3.83	3.64	10.29	14.47	3.14
0.85	1.6	74.08	15.18	3.83	4.87	13.76	9.46	4.17
0.9	1.4	71.14	22.66	3.83	7.14	20.18	3.81	5.74

Table 3 Top desalination performance of the HPPDS at different dehumidification effectiveness

ε_d	$MFRR$	$m_{w,d}$ (kgh^{-1})	$m_{w,e}$ (kgh^{-1})	COP	W_c (kW)	Q_e(kW)	Q_h (kW)	GOR
0.8	1.6	70.47	19.73	3.83	6.22	17.58	8.30	4.16
0.85	1.6	74.08	15.18	3.83	4.87	13.76	9.46	4.17
0.9	1.6	77.56	10.79	3.83	3.53	9.97	10.62	4.18

Table 4 Top desalination performance of the HPPDS at different inlet humidity of the ambient air

φ_{a1}	$MFRR$	$m_{w,d}$ (kgh^{-1})	$m_{w,e}$ (kgh^{-1})	COP	W_c (kW)	Q_e(kW)	Q_h (kW)	GOR
0.3	1.6	75.25	16.37	3.83	5.22	14.76	7.13	4.96
0.5	1.6	74.08	15.18	3.83	4.87	13.76	9.46	4.17
0.7	1.72	75.99	11.62	3.83	3.77	10.65	11.71	3.79

Table 5 Top desalination performance of the HPPDS at different pressure ratios of the compressor

PR	$MFRR$	$m_{w,d}$ (kgh^{-1})	$m_{w,e}$ (kgh^{-1})	COP	W_c (kW)	Q_e(kW)	Q_h (kW)	GOR
3.5	1.4	59.77	11.52	4.38	3.16	10.68	10.07	3.62
4	1.6	74.08	15.18	3.83	4.87	13.76	9.46	4.17
4.5	1.8	87.01	19.52	3.41	7.18	17.27	8.46	4.54

Table 6 Top desalination performance of the HPPDS at different PTD_{con}

PTD_{con} (K)	$MFRR$	$m_{w,d}$ (kgh^{-1})	$m_{w,e}$ (kgh^{-1})	COP	W_c (kW)	Q_e(kW)	Q_h (kW)	GOR
5	1.8	85.44	17.68	3.83	5.57	15.74	9.55	4.55
10	1.6	74.08	15.18	3.83	4.87	13.76	9.46	4.17
15	1.4	62.02	13.40	3.83	4.36	12.33	9.50	3.65

Table 7 Top desalination performance of the HPPDS at different TTD_e

TTD_e (K)	$MFRR$	$m_{w,d}$ (kgh^{-1})	$m_{w,e}$ (kgh^{-1})	COP	W_c (kW)	Q_e(kW)	Q_h (kW)	GOR
5	1.8	88.67	21.58	3.61	7.25	18.95	8.96	4.54
10	1.6	74.08	15.18	3.83	4.87	13.76	9.46	4.17

15	1.4	58.72	10.68	4.03	3.29	9.94	9.65	3.60

Table 8 Constants and coefficients involved in the PSO algorithm

M	N	c_1	c_2	$rand_1$	$rand_2$	ω_{min}	ω_{max}	V_{min}	V_{max}
100	100	2	2	0~1	0~1	0.5	1	-1	1

Table 9 Limit values of the prescribed decision variables

Decision variable	LL	UL
MFRR	1	10
ε_h	0.8	0.9
ε_d	0.8	0.9
PR	3.5	4.5
PTD_{con} (K)	5	15
TTD_e (K)	5	15

Table 10 Optimized desalination performance of the HPPDS within the range of the decision variables and the corresponding comparison with our previous research

	$s_{gen,h}$ (kJkg^{-1}K^{-1})	*MFRR*	$m_{w,d}$ (kgh^{-1})	$m_{w,e}$ (kgh^{-1})	*COP*	W_c (kW)	Q_e(kW)	Q_h (kW)	*GOR*
Current	≈0	2.17	118.84	31.92	3.18	12.28	26.82	0.02	8.12
He [23]	≈0	2.18	124.03	27.00	3.18	10.52	22.98	6.29	5.95

Fig. 1 Configuration schemes of the HPPDS with OAOW configurations

Fig. 2 Heat and mass transfer processes of the HPPDS with OAOW configurations

Fig. 3 Distribution of the specific entropy generation rate in the HPPDS with OAOW configurations

Fig. 4 Water production from the HPPDS with OAOW configurations

Fig. 5 Energy conversion and the relevant efficiency of the HPPDS with OAOW configurations

Fig. 6 Thermodynamic performance of the HPPDS with OAOW configurations at different effectiveness during humidification, ε_h

(a) Water production

(b) GOR

Fig. 7 Thermodynamic performance of the HPPDS with OAOW configurations at different effectiveness during dehumidification, ε_d

(a) Water production

(b) GOR

Fig. 8 Thermodynamic performance of the HPPDS with OAOW configurations at different inlet humidity, φ_{a1}

(a) Water production

(b) GOR

Fig. 9 Thermodynamic performance of the HPPDS with OAOW configurations at different pressure ratios during compression, PR

(a) Water production

(b) GOR

Fig. 10 Thermodynamic performance of the HPPDS with OAOW configurations at different pinch

temperature difference during condensation, PTD_{con}

(a) Water production

(b) GOR

Fig. 11 Thermodynamic performance of the HPPDS with OAOW configurations at different terminal temperature difference during evaporation, TTD_e

(a) Water production

(b) GOR

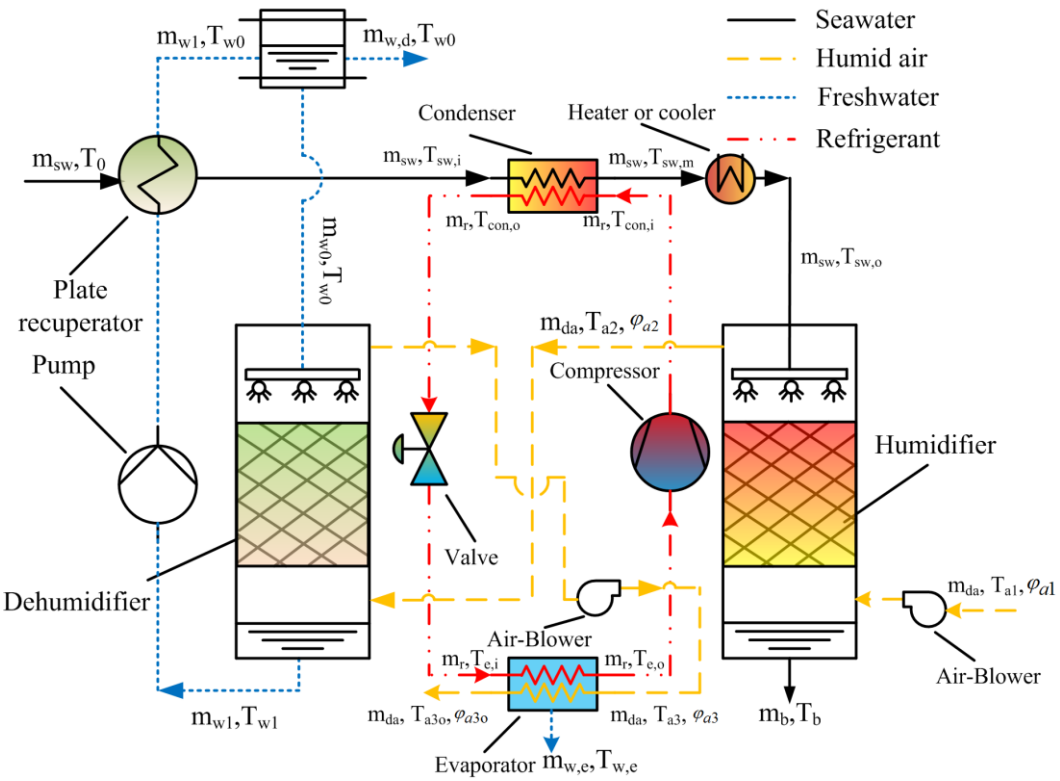

Fig. 1 Configuration schemes of the HPPDS with OAOW configurations

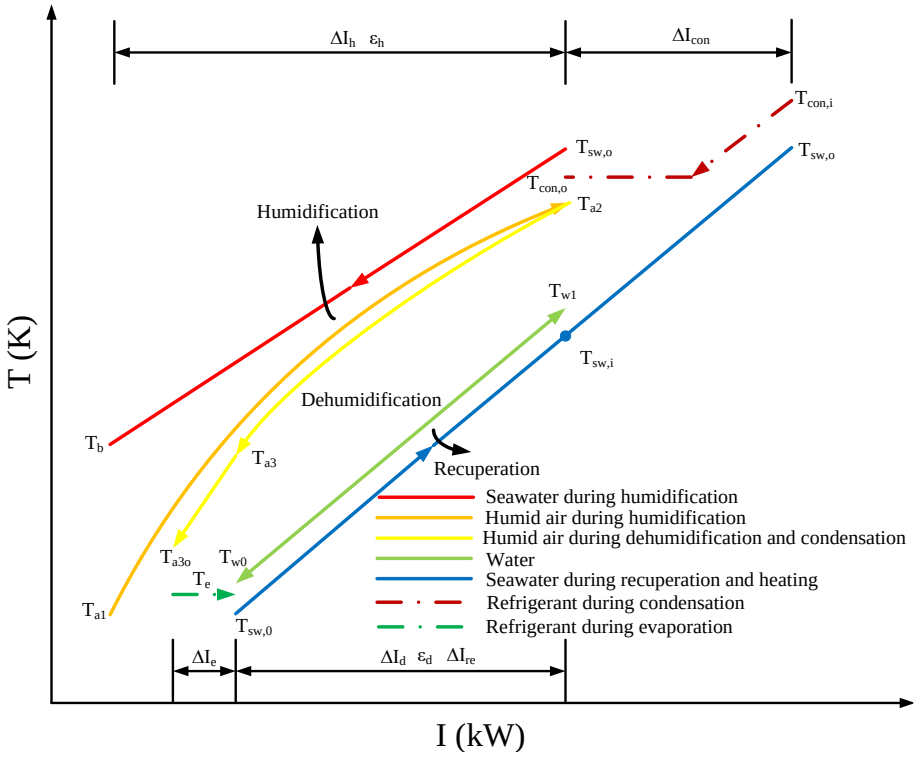

Fig. 2 Heat and mass transfer processes of the HPPDS with OAOW configurations

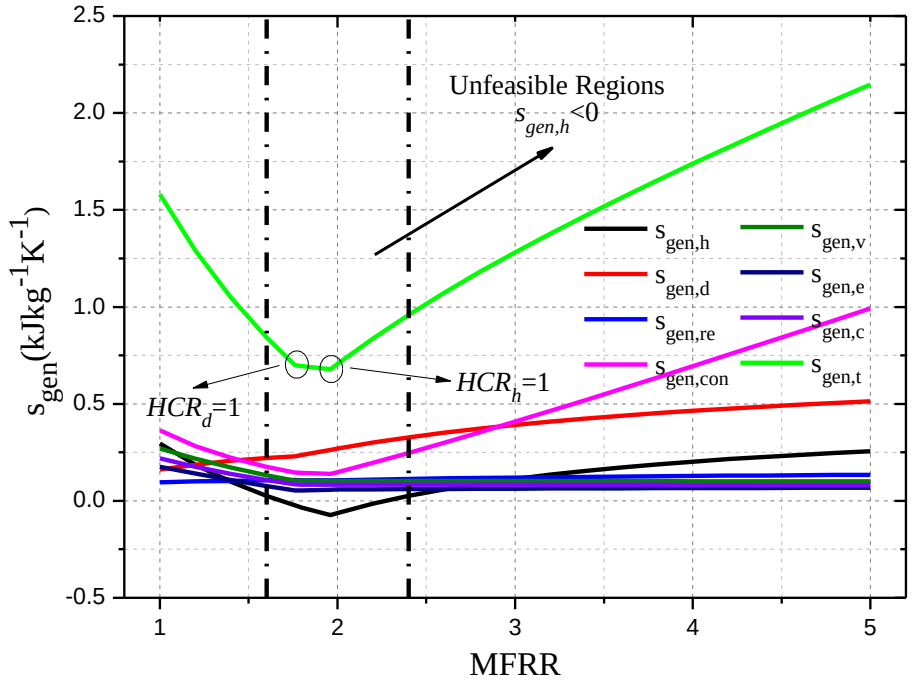

Fig. 3 Distribution of the specific entropy generation rate in the HPPDS with OAOW configurations

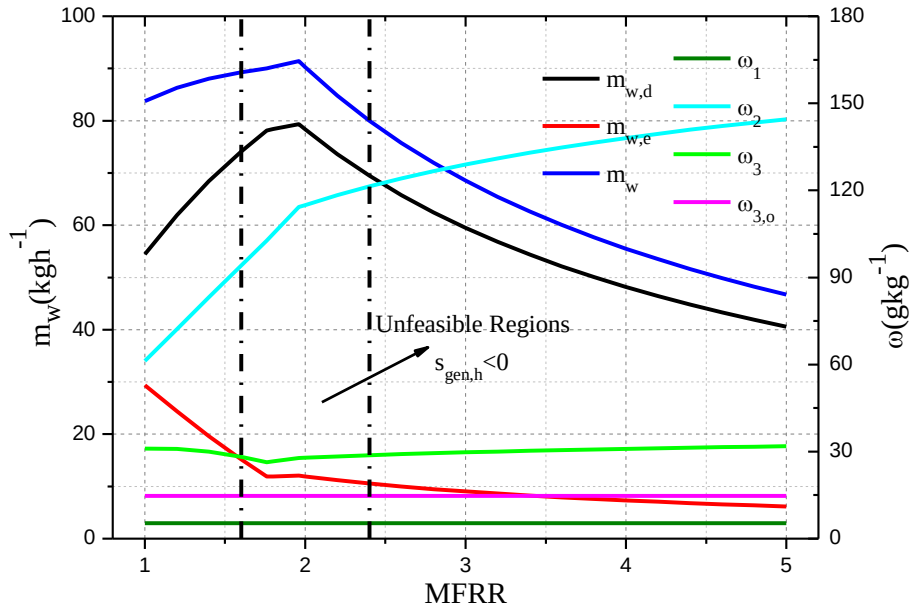

Fig. 4 Water production from the HPPDS with OAOW configurations

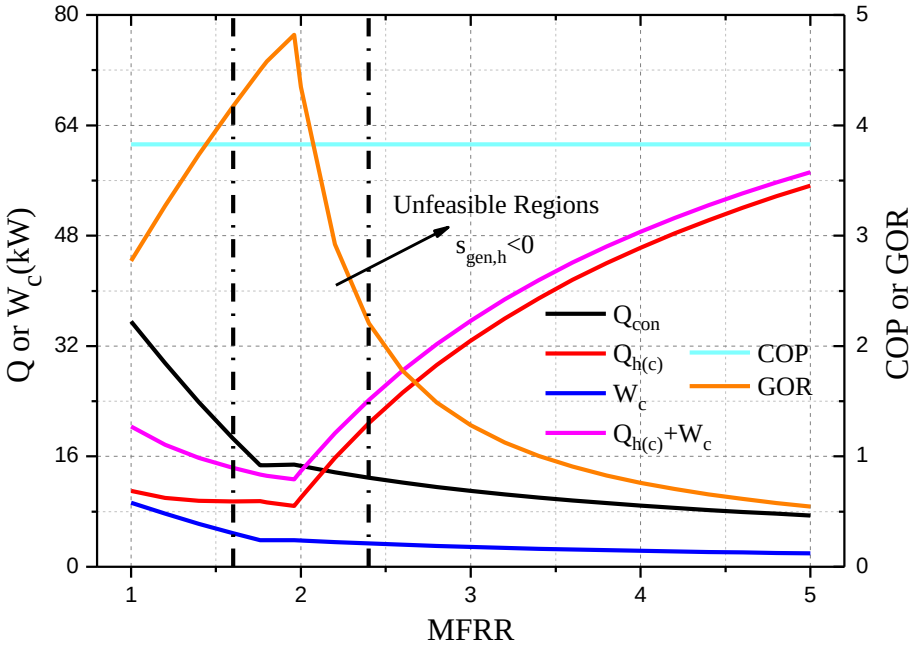

Fig. 5 Energy conversion and the relevant efficiency of the HPPDS with OAOW configurations

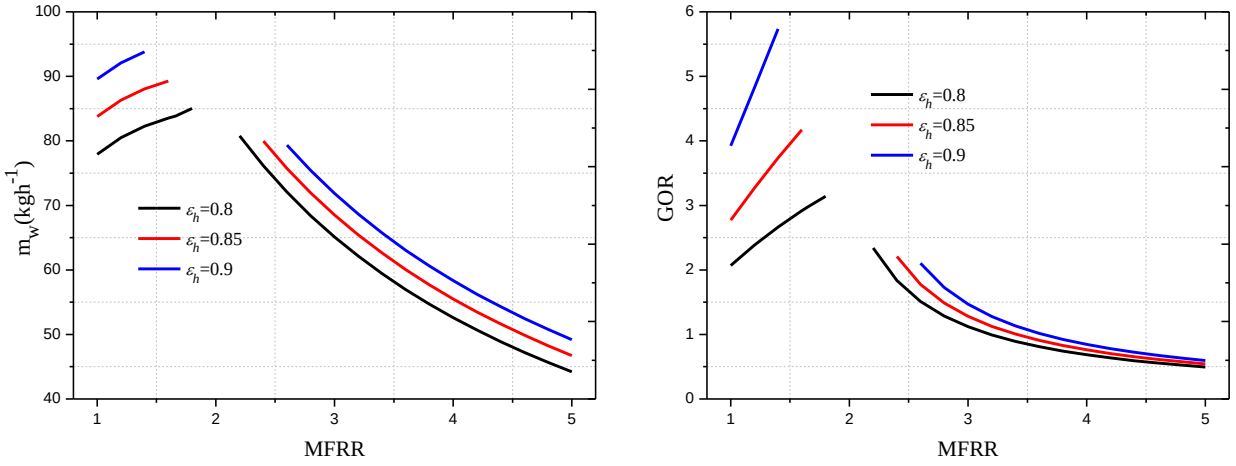

(a) Water production

(b) GOR

Fig. 6 Thermodynamic performance of the HPPDS with OAOW configurations at different effectiveness during humidification, ε_h

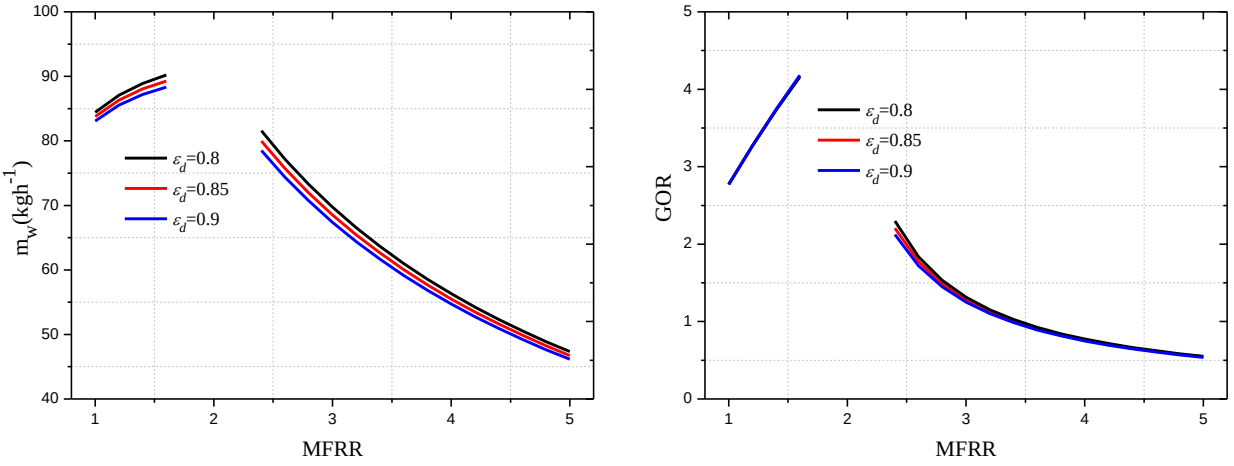

(a) Water production

(b) GOR

Fig. 7 Thermodynamic performance of the HPPDS with OAOW configurations at different effectiveness during dehumidification, ε_d

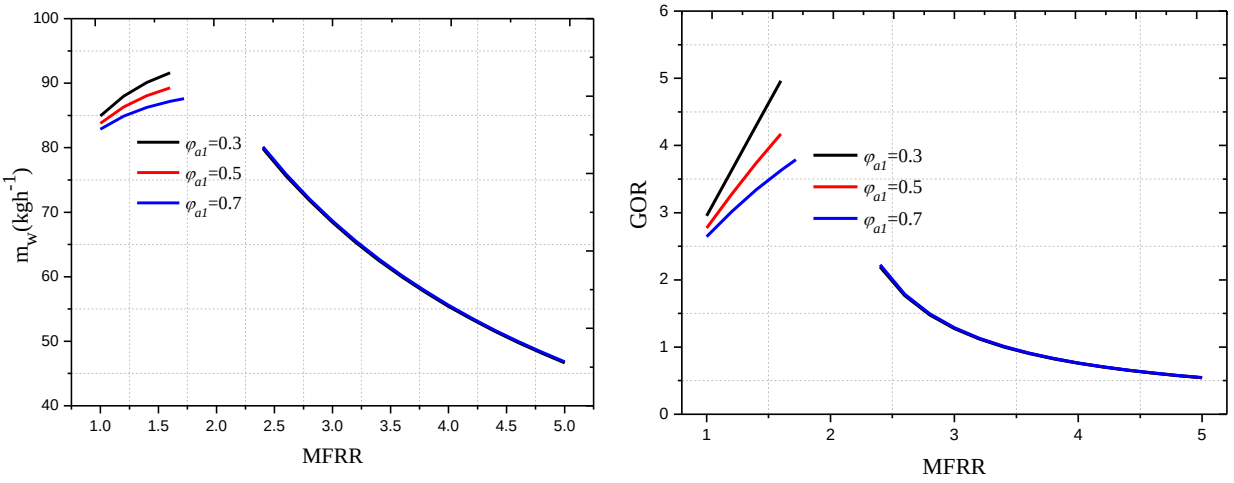

(a) Water production

(b) GOR

Fig. 8 Thermodynamic performance of the HPPDS with OAOW configurations at different inlet humidity, φ_{a1}

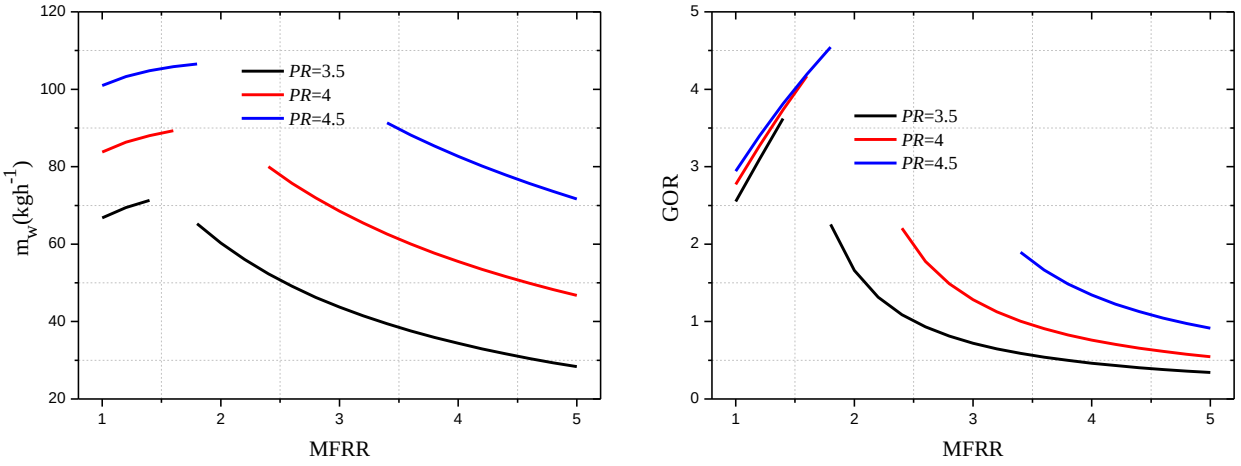

(a) Water production

(b) GOR

Fig. 9 Thermodynamic performance of the HPPDS with OAOW configurations at different pressure ratios during compression, PR

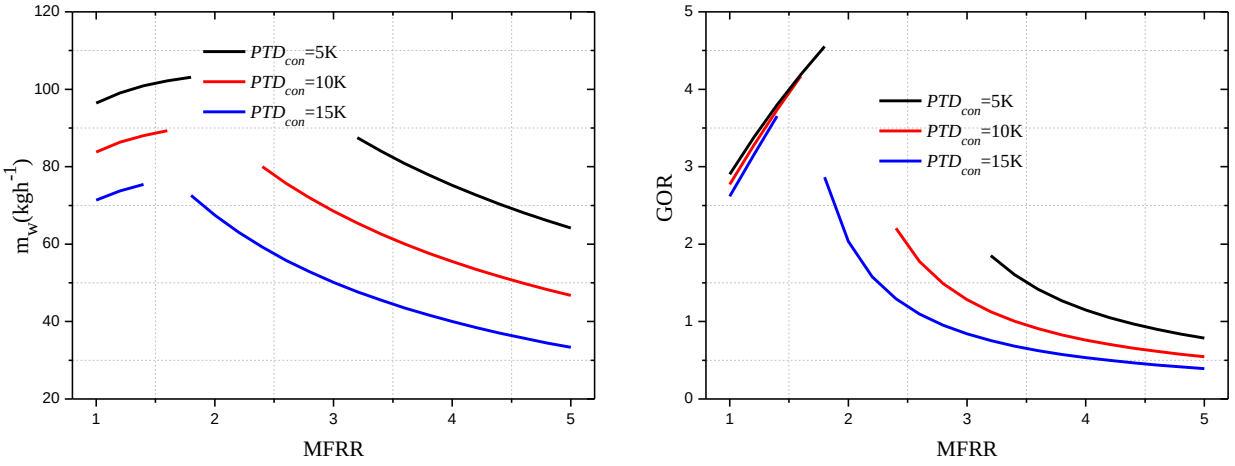

(a) Water production

(b) GOR

Fig. 10 Thermodynamic performance of the HPPDS with OAOW configurations at different pinch temperature difference during condensation, PTD_{con}

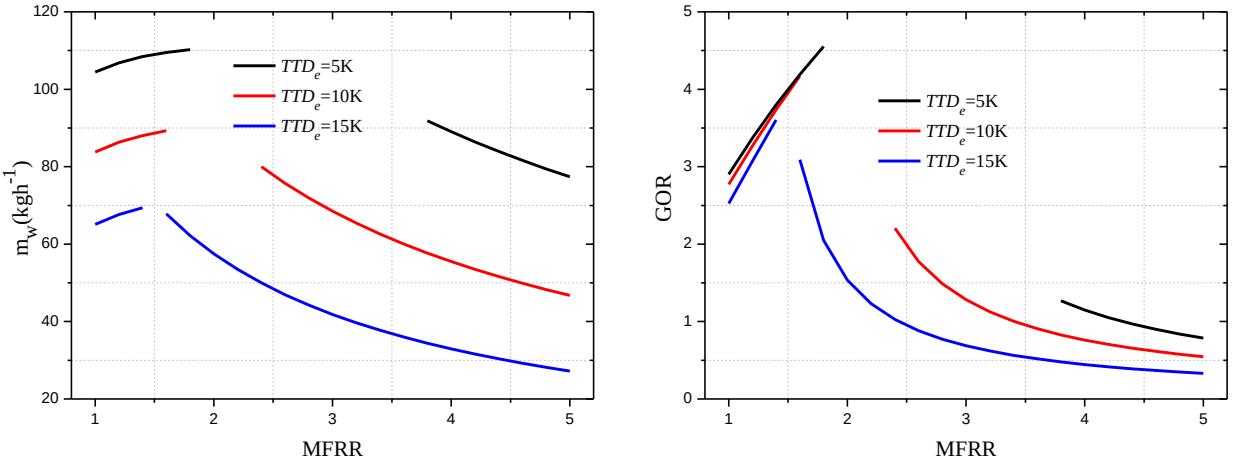

(a) Water production

(b) GOR

Fig. 11 Thermodynamic performance of the HPPDS with OAOW configurations at different terminal temperature difference during evaporation, TTD_e